The Canadian Mineralogist
Vol. 36, pp. 463-482 (1998)

MICAS FROM THE PIKES PEAK BATHOLITH AND ITS COGENETIC GRANITIC PEGMATITES, COLORADO: OPTICAL PROPERTIES, COMPOSITION, AND CORRELATION WITH PEGMATITE EVOLUTION

DANIEL E. KILE[1]

MS 408, U.S. Geological Survey, Denver Federal Center, Box 25046, Denver, Colorado 80225, U.S.A.

EUGENE E. FOORD†

MS 905, U.S. Geological Survey, Denver Federal Center, Box 25046, Denver, Colorado 80225, U.S.A.

Abstract

Optical properties are presented for 66 samples of mica covering the range from annite → biotite → zinnwaldite → ferroan lepidolite and ferroan muscovite from occurrences of granitic pegmatite (NYF type) throughout the Pikes Peak batholith (PPB) in Colorado. Chemical composition was determined for 34 of these samples. The optical data are correlated with composition, mode of occurrence, and relation to pegmatite paragenesis. Optical properties of the trioctahedral micas show a consistent trend of decreasing β index of refraction, from an average of 1.693 in annite of the host granite to 1.577 in zinnwaldite and ferroan lepidolite of the miarolitic cavities, which correlates with a progressively decreasing content of Fe. A comparison of optical and compositional data for micas from localities throughout the PPB indicates a variation in geochemical evolution among pegmatites of different districts, and between the Pikes Peak Granite and its late satellite plutons. Analyses of mica samples taken from cross-sections through individual pegmatites reveal a decrease in index of refraction and total iron that unambiguously document a progressive geochemical evolution within a given pegmatite. Such data, in addition to field evidence, indicate that micas enclosed within massive quartz are paragenetically older than those within miarolitic cavities; minerals within miarolitic cavities represent the final stages of primary crystallization. A general model of pegmatite paragenesis is proposed that hypothesizes formation of miarolitic cavities as a consequence of pegmatite configuration and inclination, as well as early crystallization of massive quartz that confines the silicate melt and volatile phase, resulting in closed-system crystallization with a concomitant increase in pressure, consequent episodic cavity-rupture events, and corresponding changes in mica composition.

Keywords: annite, biotite, iron content, paragenesis, pegmatite, index of refraction, zinnwaldite, Pikes Peak batholith, Colorado.

Sommaire

Nous présentons les propriétés optiques de 66 échantillons de mica représentant l'intervalle annite → biotite → zinnwaldite → lépidolite et muscovite ferrifères, prélevés de pegmatites granitiques de type NYF dans le batholithe de Pikes Peak, au Colorado. Nous présentons aussi des données sur la composition de 34 de ceux-ci. Les données optiques dépendent de la composition, du type de gisement, et de la relation avec les associations paragénétiques. Les échantillons de mica trioctaédriques montrent une diminution progressive de l'indice de réfraction β, d'une moyenne de 1.693 dans l'annite du granite encaissant à 1.577 dans la zinnwaldite et la lépidolite ferrifère des cavités miarolitiques, diminution qui est en corrélation avec la diminution de la teneur en Fe. Une comparaison des données optiques et compositionnelles indique une variation du degré d'évolution géochimique parmi les pegmatites des différents districts, et entre le batholithe de Pikes Peak et les plutons tardifs satellites. Pour le cas d'échantillons prélevés le long de coupes à travers des massifs individuels de pegmatite, nous documentons une diminution de l'indice β et de la teneur en Fe total qui illustre de façon non ambiguë la direction de l'évolution. De telles données, évaluées en considérant les relations de terrain, montrent que le mica piégé dans le noyau de quartz massif est antérieur au mica des cavités miarolitiques. Les minéraux de ces cavités représenteraient le stade final de cristallisation primaire. Nous décrivons ces tendances au moyen d'un modèle général de cristallisation. La formation de cavités dépend de l'attitude et l'inclinaison de la pegmatite, et la cristallisation précoce de quartz massif, qui piège le magma silicaté et la phase volatile. Il en résulte une cristallisation en système fermé, avec comme conséquences une augmentation de la pression, des ruptures épisodiques des cavités, et des changements correspondants dans la composition du mica.

(Traduit par la Rédaction)

Mots-clés: annite, biotite, teneur en Fe, paragenèse, pegmatite, indice de réfraction, zinnwaldite, batholithe de Pikes Peak, Colorado.

[1] *E-mail address*: dekile@usgs.gov
† deceased 8 January 1998.

INTRODUCTION

The Pikes Peak batholith (PPB) in central Colorado is noted for its granitic pegmatites containing small- to medium-sized miarolitic cavities (as much as 2.5 m across) that yield fine specimens of amazonitic K-feldspar, smoky quartz, goethite, topaz, fluorite, and other minerals. These occur in such well-known pegmatite-bearing areas (Fig. 1) as Devils Head, the Crystal Peak and Lake George areas that encompass the Lake George ring (LGR) complex, the Tarryall area (Spruce Grove Campground and Matucat Road) that encompasses the Redskin stock, the Wigwam Creek area (trailhead area and Sugarloaf Peak), the Sentinel Rock, Crystal Park, Cameron Cone, and Stove Mountain areas west of Colorado Springs, and the Glen Cove area on the northwest side of Pikes Peak.

Within the host granite and the graphic-textured pegmatite, crystals of the early-formed micas are unzoned, but the mica that crystallized later, within miarolitic cavities, may show distinct color zoning that becomes readily visible when the "books" of mica are separated along the {001} cleavage (Figs. 2–5). Some specimens show complex zoning (*e.g.*, Fig. 5), whereas other specimens show simple zoning, with only a few "color bands" (Figs. 3, 4), or a distinctive epitactic overgrowth (Fig. 6), in which a polycrystalline core of ferroan zinnwaldite is surrounded by a rim of monocrystalline zinnwaldite. Mica from the Wigwam Creek area is more likely to show distinct and complex color-zonation than is that from other pegmatite districts. Flakes of mica that appear to be relatively homogeneous in plane-polarized light may display a well-defined oscillatory zonation under crossed-polarized light (*e.g.*, Fig. 7), a result of slight rotation of the optic plane relative to the *b* axis. Such zones are presumably a manifestation of subtle compositional variation and concomitant structural changes. Most flakes of color-zoned mica do not show an appreciable corresponding "optical" zonation under crossed-polarized light.

There are almost no published data on optical properties of micas from the PPB, and chemical data on a limited set of micas from granitic pegmatites in the PPB have only recently been reported (Foord *et al.* 1995). These authors documented a progression in composition, with decreasing Fe and Ti and increasing Li and F, from annite in the host granite, through siderophyllite, to lithian biotite, and finally to ferroan zinnwaldite, zinnwaldite and ferroan lepidolite in miarolitic cavities.

Because the composition of micas has been shown by Foord *et al.* (1995) to be related to geochemical evolution, they are excellent indicators of the differentiation and development of miarolitic and other types of pegmatites. A correlation of index of refraction to chemical composition (especially iron content) in micas permits the use of optical properties as an efficient means of assessing such parageneses. An advantage of optical methods is that exceedingly small quantities of sample can be examined, and a visual evaluation of alteration is possible. Consequently, a comparative evaluation of the changes in optical (and compositional) properties across color zones within single crystals of mica and in micas from pegmatite cross-sections, as well as from localities throughout the PPB, allows an assessment of paragenesis of individual occurrences of pegmatite. The present study is based on an extensive suite of micas that have been well characterized as to mode of occurrence, and that represent a thorough sampling of the various occurrences of pegmatite in the Pikes Peak batholith; studies of micas from cross-sections of pegmatite bodies have not previously been reported. These samples document a close relation between the optical and chemical properties of micas and their mode of occurrence within a given pegmatite.

GEOLOGICAL SETTING AND MODE OF OCCURRENCE

The PPB is a composite, epizonal, primarily granitic (greater than 90%) to quartz monzonitic body that is exposed over an area of about 5000 km^2 in the Front Range of central Colorado. It is an anorogenic pluton of Precambrian age, approximately 1092 ± 2 to 1074 ± 3 Ma, on the basis of a recent study of U–Pb systematics (zircon) by Unruh *et al.* (1995), and represents the last of three major intrusive episodes in the Front Range of Colorado. The plutons were emplaced at successively shallower depths (Simmons *et al.* 1987, Wobus & Hutchinson 1988), and mineralogical studies by Barker *et al.* (1975), Foord & Martin (1979), and Blasi *et al.* (1984) support an epizonal emplacement of the PPB. Hawley & Wobus (1977), Wobus & Anderson (1978), Wobus (1986), and Hutchinson (1976, 1988) provided further detail on the Pikes Peak Granite.

Numerous smaller and younger intrusions of both sodic and potassic affinity (Wobus & Anderson 1978, Wobus & Hutchinson 1988) are clustered along two parallel NW–SE trends within the batholith; the most prominent of these intrusions are illustrated in Figure 1. These late plutons are shown in detail on the Denver geological map by Bryant *et al.* (1981). The sodic plutons consist of gabbro, syenite, fayalite syenite, fayalite granite, and mildly peralkaline riebeckite granite. Late potassic plutons are metaluminous to peraluminous, and compositionally similar to the Pikes Peak Granite, but are generally finer grained. The largest of these potassic plutons, the Redskin stock, is enriched in Li, Be, and Sn, and hosts topaz-bearing pegmatites as well as Be-rich greisen deposits, such as at the Boomer mine (Hawley 1969, Hawley & Wobus 1977, Desborough *et al.* 1980).

Pegmatites throughout the batholith are concentrated in fractures both in and around the late-stage plutons and large intrusive centers. Pegmatites associated with

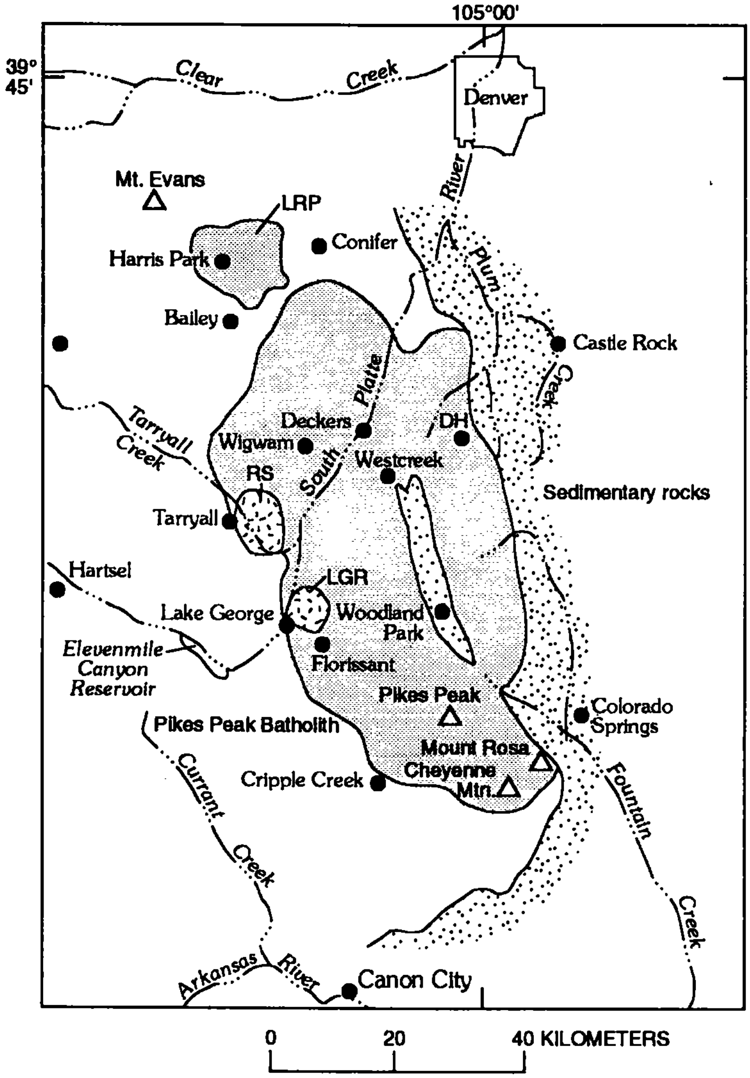

FIG. 1. Geological index-map of the Pikes Peak batholith (shaded areas), showing locations of major late-stage potassic plutons and other geographic features. LGR: Lake George ring, RS: Redskin stock, DH: Devils Head, LRP: Lone Rock pluton. Map taken from Foord *et al.* (1995).

both sodic and potassic groups are generally of the NYF (Nb–Y–F) affiliation (Černý 1991), although the youngest pegmatites show slight enrichment in Li and Rb, *i.e.*, zinnwaldite and ferroan lepidolite are present in miarolitic cavities. The pegmatites are shallow to subvolcanic; those in the southern part of the batholith host miarolitic cavities that provide the specimens of amazonitic microcline and smoky quartz for which the region is famous. Recent studies by Unruh *et al.* (1995) have elucidated the age of emplacement of late intrusive units and pegmatites of the PPB. These authors found, on the basis of $^{40}Ar/^{39}Ar$ plateau dates on riebeckite, biotite, lithian biotite, and miarolitic-cavity zinnwaldite, that the shallow-level pegmatites in the western and southern portions of the batholith were emplaced between 1062 ± 2 and 1059 ± 2 Ma, and that deeper-level bodies of pegmatite in the north (South Platte district) were emplaced between 1077 ± 2 and 1066 ± 2 Ma. In each area, U–Pb ages for the late potassic plutons are similar to those of the host

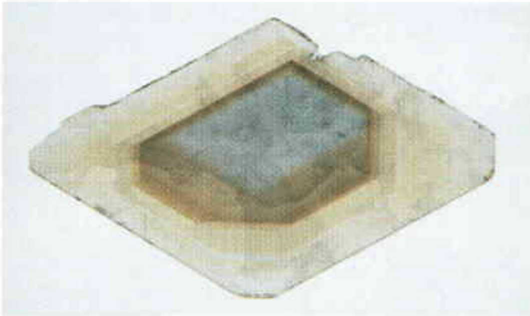

FIG. 2. Cleavage fragment of zinnwaldite (sample no. 4), 2.4 cm across, showing complex zonation, from a miarolitic cavity, Sugarloaf Peak, Wigwam Creek area. Transition from core to rim shows a decreasing β index of refraction, with the decrease being attributed to a lower Fe content. The composition of the rim corresponds to ferroan lepidolite.

FIG. 3. Cleavage fragment of zinnwaldite (sample no. 6), 2.0 cm across, showing distinct zonation, from the Lake George area, northern Lake George ring. Rim shows a substantial Ti content (0.36 wt. % TiO_2) that accounts for its dark brown color.

FIG. 4. Cleavage fragment of zinnwaldite (sample no. 3), 2.6 cm across, showing distinct zonation, from a miarolitic cavity, Sugarloaf Peak, Wigwam Creek area.

FIG. 5. Cleavage fragment of zinnwaldite (sample no. 52), 4.4 cm across, showing complex zonation, from a miarolitic cavity, Wigwam Creek trailhead area.

FIG. 6. Crystal of zinnwaldite (sample no. 54), 7 × 5.8 cm, showing distinct zoning, from a miarolitic cavity, Harris Park area (collected 1990). Transition from a polycrystalline core to a monocrystalline rim shows decreasing β index of refraction and increasing optic angle. The lighter color of the core (compared to the rim) is attributed to light scattering by a non-uniform polycrystalline texture, in spite of its higher Ti (0.30 wt.% TiO_2) relative to that in the rim (0.23 wt.% TiO_2).

Pikes Peak Granite. The ages of emplacement of the sodic plutons thus far analyzed by Unruh *et al.* (1995) are all ≤1085 ± 4 Ma.

A typical miarolitic pegmatite in the PPB is characterized by an outer zone of graphic pegmatite that shows increasingly large and elongate crystals toward the center, and a clay-filled cavity that commonly is centrally located. The "pocket stage" of pegmatite development represents the final result of extended fractional crystallization of the felsic magma (Foord & Martin 1979). Zinnwaldite crystals that formed in miarolitic cavities may be as much as 10 cm across and

FIG. 7. Cleavage fragment of zinnwaldite (sample no. 114), from a miarolitic cavity, Sentinel Rock. Shown under crossed polars, the fragment illustrates distinct optical zonation due to oscillatory rotation of the optic plane (*i.e.*, change in optic orientation with respect to *Y* and *Z*) by as much as 4°. Field of view 2.7 mm across.

show a characteristic pseudohexagonal morphology, in some cases with conspicuous zonation evident in cleaved sections. Examination of mineral intergrowths shows that zinnwaldite crystallized over an extended period in the miarolitic cavity, being contemporary with early-formed feldspars but preceding the formation of lower-temperature minerals such as fluorite and goethite. Mica crystals from miarolitic cavities in and near the Lake George ring complex are much less common than elsewhere in the PPB. This may be due either to hydrothermal alteration to vermiculite during post-mineralization activity (Foord *et al.* 1995), or to early dissolution in unstable environments in some cavities.

The central part of the pegmatite may consist partly or completely of a massive quartz core that encloses other minerals. Such quartz-filled areas within pegmatites are hereafter referred to as "quartz core" occurrences. Although this term traditionally applies to very large pegmatites that show a core of massive quartz, as in the pegmatites of the South Platte district, it is used here in an analogous sense for comparatively smaller pegmatites, in reference to the massive quartz that may comprise all or part of the central "core" of the pegmatite. The quartz is typically milky to smoky in color, with varying degrees of translucency. Mica crystals formed within a quartz core typically show an elongate, pseudohexagonal or trigonal form, commonly manifested as barrel-shaped or tapered crystals; they rarely show the distinct color zones noted in zinnwaldite from miarolitic cavities. Varying degrees of alteration to vermiculite or other clay minerals are generally evident in these crystals as well. Micas formed within the graphic pegmatite zone are typically subhedral lath-shaped crystals, and usually show some degree of alteration, as do anhedral grains of mica within the Pikes Peak Granite itself.

Methods and Instrumentation

Sixty-six mica crystals representing localities throughout the mineral-specimen-producing areas of the PPB were studied. Physical descriptions and general localities for these samples are given in Table 1. Of these samples, 38 were collected from miarolitic cavities, 10 from quartz-core occurrences, eight from graphic pegmatite, and seven from host granites. Three samples are representative of "remnant mica" that formed during early stages of miarolitic cavity crystallization and that were subsequently partly resorbed. Complete optical data were obtained for all 66 samples (including core and rim zones of ten crystals). Measured optical properties are tabulated in Table 2 for pegmatites throughout the PPB according to mode of occurrence, *i.e.*, host granite, graphic pegmatite, quartz core, remnant mica, and miarolitic cavity. Thirty-four samples were quantitatively analyzed for major constituents; there was insufficient sample to permit analyses for Li or FeO/Fe_2O_3. Table 3 shows results of quantitative analyses for selected samples, whereas Table 4 gives empirical formulas of the micas. Identical areas from zoned micas were used for both optical and compositional analyses. Nine samples represent mica collected from different units within a single pegmatite and adjacent host granite that was excavated in 1986, whereas 19 others represent mica collected from cross-sections through six other pegmatites or host granites (or both). Table 5 summarizes optical properties and compositions of the micas representing cross-sections through individual pegmatites.

Optical data were determined using a conventional petrographic microscope and calibrated immersion oils. Two of the indices, ß and γ, were determined by grain mount on an approximately centered Bxa figure; α was determined using spindle stage methods to attain proper orientation of the *X* vibration direction. Observation of the Becke line for determination of indices of refraction in white light proved to be problematic because of unfavorable geometry of the grains, pleochroism, alteration, and inclusions. Movement of the Becke line in ambiguous situations was confirmed with a 589 nm interference filter. Samples showing considerable alteration (*e.g.*, numbers 44, 63, and 68) were carefully examined to locate transparent grains showing little or no alteration for use in determination of the indices of refraction. Such unaltered portions of mica flakes yielded consistent results, in agreement with Peikert (1963), who noted that a moderate degree of chloritization did not affect the indices. Determination of the indices of refraction in the case of lighter-colored micas (zinnwaldite and some biotite) was relatively straightforward, and the error is given as ±0.002, whereas determination of the indices of the darker and more pleochroic samples,

TABLE 1. DESCRIPTION OF SELECTED MICA SAMPLES FROM THE PIKES PEAK BATHOLITH

Sample	Description
1.	Pale brown zinnwaldite from a miarolitic cavity, northeastern LGR.
4.	Zoned mica (Fig. 2) with gray zinnwaldite core and pale brown ferroan lepidolite rim, from a miarolitic cavity, Sugarloaf Peak, Wigwam Creek area. Associated with medium-blue microcline (amazonite).
6.	Zoned ferroan zinnwaldite with gray core and brown rim (Fig. 3); from a miarolitic cavity, northern LGR.
7.	Zoned, pale brown zinnwaldite from a miarolitic cavity near Devils Head. Associated with topaz, smoky quartz, and microcline.
28.	Dark brown-to-black, tapered, hexagonal biotite from quartz core (1978), northeast of the LGR. Associated with samples 90 and 92.
33.	Dark brown biotite enclosed in massive quartz (1986), from a pegmatite in coarse-grained Pikes Peak Granite (Ypc), LGR; associated with samples 56, 72-74, 77, 87 and 88.
38.	Lustrous, dark brown-to-black, hexagonal biotite enclosed in massive quartz, northern LGR (1978); sample adjacent to no. 44. Associated with medium-to-dark blue microcline (amazonite).
43.	Pseudohexagonal brown zinnwaldite, 1.4 cm across, from a miarolitic cavity, northern LGR; associated with microcline (variety amazonite) and smoky quartz.
44.	Biotite showing alteration, with bronze color and submetallic luster. From graphic pegmatite (1978), northern LGR; sample adjacent to no. 38.
47.	Black, lustrous biotite from quartz core, north of the LGR. Associated with microcline.
51.	Pale-brown zinnwaldite showing indistinct zoning, from a miarolitic cavity near the Wigwam Creek trailhead. Associated with pale-blue microcline (amazonite), smoky quartz, and albite (sample 24-1, Foord *et al.*, 1995).
52.	Pale-to-medium brown, distinctly zoned zinnwaldite, 4.4 cm across (Fig. 5), from a miarolitic cavity near the Wigwam Creek trailhead.
53.	Vivid bluish-green lithian biotite from quartz core near the Wigwam Creek trailhead. Associated with quartz, microcline, and albite.
54.	Distinctly zoned, hexagonal zinnwaldite with a brown polycrystalline core that has a silvery-submetallic luster, and a dark-brown monocrystalline rim (Fig. 6). From a miarolitic cavity collected near Harris Park in 1992; associated with pale-to-medium blue microcline (amazonite).
55.	Zoned zinnwaldite, with a light-brown core and brown rim; from a miarolitic cavity, Sugarloaf Peak, Wigwam Creek area (samples 1a and 1b, Foord *et al.*, 1995).
56.	Hexagonal, lustrous dark brown-to-black zinnwaldite from a miarolitic cavity (1986), associated with medium-blue microcline (amazonite), smoky quartz, and albite. From a pegmatite in coarse-grained (Ypc) Pikes Peak Granite, LGR; associated with samples 33, 72-74, 77, 87 and 88.
60.	Pale brown-to-gray miarolitic cavity zinnwaldite, 2.6 cm across, from the Devils Head area.
62.	Partly altered, dark brown-to-black biotite, from graphic pegmatite north of LGR; sample adjacent to no. 64.
63.	Lustrous, black, anhedral annite from coarse-grained Pikes Peak Granite (Ypc), northeastern LGR.
64.	Irregular, hexagonal biotite from quartz core; partly altered, with submetallic bronze color and submetallic luster, from locality north of the LGR. Associated with pale microcline (variety amazonite); sample adjacent to no. 62.
65.	Relatively unaltered, dark brown-to-black biotite in graphic pegmatite, north of the LGR.
66.	Olive-green lithian biotite from quartz core (1972), eastern LGR. Associated with medium-blue microcline (amazonite); sample adjacent to no. 67.
67.	Anhedral, dark brown-to-black biotite, from graphic pegmatite (1972), eastern LGR; sample adjacent to no. 66.
68.	Anhedral dark brown-to-black biotite, from medium-grained Pikes Peak Granite (Ypm), southwestern LGR.
69.	Very pale brown-to-gray, nearly colorless ferroan lepidolite, from a miarolitic cavity northwest of Crystal Peak, eastern LGR. Associated with pale-to-medium blue microcline (amazonite, with microcline overgrowth), quartz, and albite (sample 21, Foord *et al.*, 1995).
72.	Remnant ferroan zinnwaldite from an irregular cavity (remaining after partial dissolution of early mica) alongside the base of a miarolitic-cavity microcline (amazonite) crystal, from the 1986 pegmatite in coarse-grained Pikes Peak Granite (Ypc), LGR. Associated with samples 33, 56, 73, 74, 77, 87 and 88.
73.	Remnant ferroan zinnwaldite from an elongate depression (remaining after partial dissolution of early mica) showing part of a hexagonal outline in massive quartz and microcline (variety amazonite) from the wall of a miarolitic cavity. From the 1986 pegmatite in coarse-grained Pikes Peak Granite (Ypc), LGR. Associated with samples 33, 56, 72, 74, 77, 87 and 88.
74.	Intergrown crystal of brown zinnwaldite from miarolitic cavity of 1986 pegmatite in coarse-grained Pikes Peak Granite (Ypc), LGR. Associated with samples 33, 56, 72, 73, 77, 87 and 88.
77.	Euhedral, dark brown-to-black zinnwaldite showing distinct core and rim zones; partly enclosed by smoky quartz crystal. From the 1986 pegmatite, coarse-grained Pikes Peak Granite (Ypc), LGR; associated with samples 33, 56, 72-74, 87 and 88.
83.	Euhedral, colorless-to-gray muscovite, 1 mm across, on microcline. From a miarolitic cavity near the Spruce Grove Campground, Tarryall area.
87.	Anhedral, lath-shaped, dark brown biotite from fine-grained graphic pegmatite (1986). Associated with samples 33, 56, 72-74, and 88.
88.	Lustrous, black, anhedral annite from coarse-grained Pikes Peak Granite (Ypc), LGR, near the 1986 pegmatite. Associated with samples 33, 56, 72-74, and 87.
90.	Lustrous, black, anhedral annite from coarse-grained Pikes Peak Granite (Ypc), northeast of the LGR; associated with samples 28 and 92.
92.	Anhedral biotite, about 1 cm across, from graphic pegmatite adjacent to the 1978 quartz core occurrence northeast of the LGR; associated with samples 28 and 90.
98.	Irregular, black, lustrous, lath-shaped biotite from graphic pegmatite, Sugarloaf Peak, Wigwam Creek area. Associated with samples 99, 102, and 136.
99.	Anhedral black annite about 6 mm across from medium-to-coarse-grained, hastingsite-bearing granite, Sugarloaf Peak, Wigwam Creek area. Associated with samples 98, 102, and 1366.
102.	Lustrous, pale brown, trigonal zinnwaldite embedded in massive quartz, with euhedral microcline (pale amazonite), Sugarloaf Peak, Wigwam Creek area. Associated with samples 98, 99, and 136.
103.	Dark brown-to-black crude hexagonal biotite from a quartz core occurrence, Crystal Park area. Associated with microcline (variety amazonite).
104.	Pale gray-to-brown pseudohexagonal zoned zinnwaldite, 5 cm across, from a miarolitic cavity in the Crystal Park area. Associated with microcline (variety amazonite) and smoky quartz.
106.	Distinctly zoned zinnwaldite with polycrystalline core and monocrystalline rim, from a miarolitic cavity, Crystal Park area.
112.	Small, pale brown muscovite from a miarolitic cavity near Spruce Grove Campground, Tarryall area. Associated with microcline, smoky quartz and fluorite.
114.	Hexagonal, pale gray-to-brown, zoned ferroan lepidolite (Fig. 7) with a polycrystalline core, 4.5 cm across. From a miarolitic cavity near Sentinel Rock.
115.	Dark brown, zoned zinnwaldite from a miarolitic cavity in the Sentinel Rock area.
117.	Mica separate from Redskin Granite (outer zone, Redskin stock) near Matucat road, Tarryall area.
119.	Large anhedral gray-green lithian biotite (4.8 cm across) from a quartz core occurrence at the Wigwam Creek trailhead, near sample 120.
120.	Mica separate (annite) from the Wigwam trailhead, near sample 119.
124.	Pale brown zinnwaldite from a miarolitic cavity, Stove Mountain area; associated with medium-blue microcline (amazonite), smoky quartz, topaz, fluorite and cookeite.
125.	Dark brown, lath-shaped biotite from graphic pegmatite, Crystal Park area; partly altered to a bronze, submetallic luster. Associated with microcline (variety amazonite) and smoky quartz.
126.	Pale brown zinnwaldite, 3.5 cm across, from a miarolitic cavity, Cameron Cone area; associated with microcline.
127.	Medium-to-light brown, distinctly zoned zinnwaldite, 4 cm across, from a miarolitic cavity, Stove Mountain area.
128.	Dark brown, zoned zinnwaldite, 2.4 cm across, from a miarolitic cavity, Cameron Cone area.
129.	Zoned, colorless muscovite, 3.5 mm across, on a white microcline crysta from a miarolitic cavity, Spruce Grove Campground, Tarryall area; associated with fluorite and smoky quartz.
130.	Brown pseudohexagonal zinnwaldite, 2.6 cm across, from a miarolitic cavity, Devils Head area. Associated with microcline, albite, smoky quartz, and fluorite.
132.	Pale brown-to-gray pseudohexagonal miarolitic cavity zinnwaldite, Harris Park area. Associated with microcline and smoky quartz.
133.	Zoned crystal, 9 cm across, with a pale-to-medium brown zinnwaldite rim and gray-green lithian biotite core. From a miarolitic cavity, Harris Park area; associated with microcline and smoky quartz.
136.	Zoned pseudohexagonal zinnwaldite, 5 cm across, from a miarolitic cavity, Sugarloaf Peak, Wigwam Creek area; associated with medium-blue microcline (amazonite), smoky quartz, and manganocolumbite. Mica crystal composed of a monocrystalline pale brown-to-gray rim, light-to-dark brown zoned interior, and polycrystalline pale brown-to-gray base that is partly enclosed by graphic pegmatite wallrock that borders the miarolitic cavity. Associated with samples 98, 99, and 102.
137.	Pseudohexagonal, gray-to-pale-brown mica, 2.8 cm across, from a miarolitic cavity, southwestern LGR. Associated with smoky quartz, microcline, and albite (sample 86-25, Foord *et al.*, 1995).
140.	Lustrous, pale, light-brown, and gray-zoned zinnwaldite, 5.2 cm across, from a miarolitic cavity in the medium-grained granite (Ypm), LGR. Associated with microcline (variety amazonite) and smoky quartz.
143.	Pseudohexagonal, light-brown zinnwaldite, 3 cm across, with distinct polycrystalline core, from a miarolitic cavity near Harris Park.
146.	Pseudohexagonal muscovite, 3 mm across, on smoky quartz crystal from a miarolitic cavity near Glen Cove. Associated with microcline (pale amazonite).
147.	Pseudohexagonal muscovite, 6 mm across, on a microcline crystal from a miarolitic cavity near Glen Cove. Associated with smoky quartz.
148.	Brown, lustrous pseudohexagonal miarolitic cavity zinnwaldite, 2.5 cm across, from a pegmatite in medium-grained granite (Ypm), northern LGR. Associated with smoky quartz and medium-to-dark blue microcline (amazonite).
149.	Pseudohexagonal zinnwaldite, zoned brown-to-gray, 5.5 cm across, from a miarolitic cavity, Crystal Park area. Associated with microcline and smoky quartz.
150.	Pseudohexagonal, pale-brown zinnwaldite, 5.2 cm across, showing faint zonation. From a miarolitic cavity, Crystal Park area. Associated with microcline and smoky quartz.
153.	Remnant, polycrystalline ferroan zinnwaldite from an irregular hexagonal cavity (remaining after partial dissolution of early mica) at the base of euhedral microcline (variety amazonite) crystals within a miarolitic cavity. From a pegmatite in medium-grained granite (Ypm), northern LGR. Associated with microcline (amazonite), smoky quartz, and rutile.
159.	Pseudohexagonal, pale brown, miarolitic cavity zinnwaldite, 4.5 cm across, showing distinct zonation. From a pegmatite in coarse-grained granite (Ypc), northern LGR. Associated with microcline (amazonite) and smoky quartz.

Notes: Dates indicate the year collected, and correspond to dates given in Table 2. LGR: Lake George ring.

TABLE 2. OPTICAL DATA FOR MICAS FROM THE PIKES PEAK BATHOLITH

I. Host Granite; annite, biotite

number	locality	$2V_x$	n_α	n_β	n_γ	δ
63	LGR, northeastern; Ypc	21.0	1.611	1.695	1.695	0.084
68	LGR, southwestern; Ypm	11.0	1.610	1.684	1.684	0.074
88	LGR, Ypc (1986)	15.1	1.612	1.705	1.705	0.093
90	LGR, northeast of; Ypc (1978)	16.1	1.611	1.703	1.705	0.094
117	Redskin Granite, Tarryall area	7.8	1.597	1.663	1.663	0.066
99	Wigwam Cr. area, Sugarloaf Pk.; medium- to coarse-grained granite	9.8	1.611	1.697	1.697	0.086
120	Wigwam Cr. trailhead; Ypc	12.7	1.615	1.702	1.702	0.087
			average =	1.693		

II. Graphic Pegmatite; biotite

number	locality	$2V_x$	n_α	n_β	n_γ	δ
125	Crystal Park area	7.0	1.585	1.639	1.639	0.054
44	LGR, northern (1978)	12.2	nd	1.655	1.655	nd
67	LGR, eastern (1972)	10.0	1.583	1.641	1.641	0.058
87	LGR, Ypc (1986)	6.6	1.599	1.671	1.671	0.072
92	LGR, northeast of (1978)	10.0	1.591	1.657	1.657	0.066
62	north of LGR	2.8	nd	1.687	1.687	nd
65	north of LGR	8.5	1.577	1.619	1.619	0.042
98	Wigwam Cr. area, Sugarloaf Pk.	4.6	1.599	1.659	1.659	0.060
			average =	1.654		

III. Quartz Core; biotite, ferroan zinnwaldite

number	locality	$2V_x$	n_α	n_β	n_γ	δ
103	Crystal Park area	6.4	1.563	1.603	1.603	0.040
28	LGR, northeast of (1978)	5.8	1.595	1.653	1.653	0.058
33	LGR, Ypc (1986)	9.4	1.594	1.667	1.667	0.073
38	LGR, northern (1978)	4.8	1.587	1.623	1.623	0.036
66	LGR, eastern (1972)	14.5	1.583	1.637	1.637	0.054
47	north of LGR	13.1	1.583	1.636	1.637	0.054
64	north of LGR	10.0	nd	1.675	1.675	nd
102	Wigwam Cr., Sugarloaf Pk. -core	18.0	1.555	1.585	1.586	0.031
102	Wigwam Cr., Sugarloaf Pk. -rim	23.3	1.555	1.583	1.585	0.030
53	Wigwam Cr., trailhead area	3.2	1.574	1.617	1.617	0.043
119	Wigwam Cr. area, trailhead	4.3	1.570	1.611	1.611	0.041
			average =	1.631		

IV. Remnant, Early Miarolitic Cavity Mica; ferroan zinnwaldite

number	locality	$2V_x$	n_α	n_β	n_γ	δ
72	LGR, Ypc (1986)	4.4	1.559	1.597	1.597	0.038
73	LGR, Ypc (1986)	4.9	1.565	1.602	1.602	0.037
153	LGR, Ypc	12.1	1.559	1.593	1.594	0.035
			average =	1.597		

V. Miarolitic Cavity; ferroan zinnwaldite, zinnwaldite, ferroan lepidolite

number	locality	$2V_x$	n_α	n_β	n_γ	δ
126	Cameron Cone	31.7	1.543	1.567	1.569	0.026
128	Cameron Cone	32.5	1.560	1.589	1.591	0.031
149	Crystal Park area	28.2	1.553	1.580	1.581	0.028
150	Crystal Park area	30.8	1.549	1.575	1.577	0.028
104	Crystal Park area	29.1	1.553	1.581	1.583	0.030
106	Crystal Park area -core	29.4	1.555	1.583	1.584	0.029
106	Crystal Park area -rim	28.7	1.551	1.580	1.581	0.030
7	Devils Head	30.4	1.553	1.585	1.587	0.034
60	Devils Head	32.5	1.559	1.584	1.587	0.028
130	Devils Head	29.7	1.551	1.577	1.578	0.027
1	LGR, northeastern; Ypc	27.5	1.551	1.577	1.578	0.027
6	LGR, northern; Ypc -core	4.4	1.561	1.601	1.601	0.040
6	LGR, northern; Ypc -rim	3.8	1.567	1.607	1.607	0.040
43	LGR, northern; Ypc	30.5	1.553	1.583	1.585	0.032
56	LGR, Ypc (1986)	27.3	1.557	1.587	1.591	0.034
69	LGR, eastern; Ypc (Fe lepidolite)	31.0	1.540	1.563	1.565	0.025
74	LGR, Ypc (1986)	24.4	1.559	1.586	1.588	0.029
77	LGR, Ypc -core (1986)	14.0	1.559	1.599	1.599	0.040
77	LGR, Ypc -rim (1986)	26.4	1.557	1.589	1.589	0.032
137	LGR, southwestern	29.8	1.551	1.581	1.583	0.032
140	LGR, Ypm -rim	26.1	1.556	1.590	1.591	0.035
148	LGR, northern; Ypm	26.1	1.551	1.579	1.581	0.030
159	LGR, Ypc -rim	27.3	1.550	1.577	1.579	0.029
54	Harris Park area (1992) -core	8.0	1.551	1.585	1.585	0.034
54	Harris Park area (1992) -rim	29.2	1.557	1.577	1.579	0.022
132	Harris Park area	30.1	1.549	1.576	1.577	0.028
133	Harris Park area -core	4.6	1.569	1.609	1.609	0.040
133	Harris park area -rim	28.7	1.557	1.587	1.588	0.031
143	Harris Park area -rim	28.5	1.554	1.579	1.580	0.026
114	Sentinel Rock -core	32.4	1.547	1.569	1.571	0.024
114	Sentinel Rock -rim (Fe lepidolite)	32.9	1.541	1.563	1.564	0.023
115	Sentinel Rock	32.3	1.547	1.572	1.575	0.028
124	Stove Mountain	30.2	1.553	1.577	1.579	0.026
127	Stove Mountain	32.3	1.547	1.573	1.575	0.028
4	Wigwam Cr., Sugarloaf Pk.-core	27.0	1.551	1.575	1.579	0.028
4	Wigwam Cr., Sugarloaf Pk.-rim (Fe lepidolite)	27.0	1.544	1.567	1.569	0.025
55	Wigwam Cr., Sugarloaf Pk -core	29.2	1.548	1.572	1.574	0.026
55	Wigwam Cr., Sugarloaf Pk.-rim	26.5	1.547	1.569	1.570	0.023
136	Wigwam Cr., Sugarloaf Pk.; polycrystalline base	23.5	1.557	1.586	1.587	0.030
136	Wigwam Cr., Sugarloaf Pk.; interior light brown zone	28.9	1.547	1.573	1.577	0.030
136	Wigwam Cr., Sugarloaf Pk.; gray rim	28.8	1.547	1.569	1.571	0.024
51	Wigwam Cr., trailhead area -core	25.2	1.551	1.579	1.582	0.031
51	Wigwam Cr., trailhead area -rim	26.5	1.549	1.575	1.577	0.028
52	Wigwam Cr., trailhead area	28.4	1.553	1.581	1.583	0.030
			average =	1.579		

VI. Miarolitic Cavity; muscovite

number	locality	$2V_x$	n_α	n_β	n_γ	δ
83	Spruce Grove C.G., Tarryall area	31.4	1.564	1.597	1.599	0.035
112	Spruce Grove C.G., Tarryall area	30.9	1.564	1.597	1.599	0.035
129	Spruce Grove C.G., Tarryall area	36.6	1.558	1.591	1.592	0.034
146	Glen Cove	40.7	1.567	1.595	1.599	0.032
147	Glen Cove	40.5	1.568	1.597	1.599	0.031
			average =	1.595		

* listed in alphabetical order by locality. Notes: 1. Error in the measurement of the indices of refraction are ±0.002 for values below 1.650, ±0.004 for values above 1.650. 2. The value of $2V_x$ was obtained by calculation using Mallard's method ($D = Kn_\beta \sin V$). 3. Mica samples taken from the same geographic locality are from separate bodies of pegmatite except where annotated with a date; these mica samples are from different locations within the specified part of the pegmatite. 4. Abbreviations: nd: not determined, LGR: Lake George ring, Ypc: coarse-grained Pikes Peak Granite, Ypm: medium-grained Pikes Peak Granite. 5. The average n_β of miarolitic cavity micas was calculated from rim samples where applicable. 6. Fe-lepidolite: ferroan lepidolite.

i.e., those having indices above approximately 1.650, was more ambiguous, and consequently these measurements have errors of ± 0.004.

The optic axial angle was determined by Mallard's method, using an ocular micrometer; $2V_x$ was calculated from $D = Kn_\beta \sin V$. The angle of rotation of the optic plane in a zoned mica (sample 114) was determined from a stereonet plot derived from universal stage measurements. The structure (*i.e.*, dioctahedral – trioctahedral) of selected samples was determined by optic plane orientation relative to [010] using universal stage methods. Polytype was also ascertained for three of these samples (114, 129, and 147) by X-ray diffraction (XRD) using a Siemens Kristalloflex 805 operating at 40 kV, 25 mA, or a Philips XRD 3000 generator operating at 40 kV, 25 mA (Use of trade names is for identification purposes only and does not constitute endorsement by the U.S. Geological Survey). A thorough discussion of optical

TABLE 3. COMPOSITIONAL DATA FOR SELECTED MICAS FROM THE PIKES PEAK BATHOLITH

number	locality	SiO_2	Al_2O_3	TiO_2	FeO	MnO	MgO	Li_2O	CaO	Na_2O	K_2O	F	-O=F	Total
I. Host Granite; annite, biotite														
63	LGR, NE	34.6	12.9	4.00	32.8	0.53	2.29	0.38	0.00	0.06	9.0	0.9	0.36	97.1
68	LGR, SW	36.3	9.8	2.37	34.9	0.81	0.14	0.87	0.00	0.06	9.0	3.5	1.46	96.3
88	LGR, 1986	33.4	12.6	3.96	33.3	0.56	1.75	0.03	0.11	0.05	8.9	0.6	0.27	95.0
117	RSG, Tarryall	33.9	17.2	2.43	28.5	1.14	0.77	0.18	0.00	0.15	9.1	2.7	1.14	94.5
99	Wigwam Cr., SP	34.6	12.2	3.84	34.2	0.63	1.21	0.38	0.00	0.04	9.0	0.7	0.29	96.5
II. Graphic Pegmatite; biotite														
125	Crystal Park area	37.3	13.4	0.94	29.9	1.45	0.01	1.15	0.00	0.10	8.9	5.7	2.42	96.5
67	LGR, 1972	38.1	18.6	0.91	24.0	0.90	0.26	1.38	0.01	0.08	9.0	3.8	1.61	95.5
87	LGR, 1986	35.6	13.2	2.92	31.0	0.73	0.91	0.67	0.00	0.04	8.9	2.6	0.84	95.8
92	LGR, NE, 1978	37.3	13.1	1.17	30.9	0.94	0.08	1.15	0.00	0.08	8.8	3.9	1.62	95.9
65	N of LGR	39.0	1.55	1.55	21.5	0.59	0.96	1.64	0.00	0.14	9.3	4.2	1.77	96.1
98	Wigwam Cr., SP	35.0	13.4	1.52	33.6	1.35	0.00	0.49	0.00	0.10	8.8	3.5	1.49	96.3
III. Quartz Core; biotite														
103	Crystal Park area	40.3	17.8	0.53	21.4	0.77	0.20	2.01	0.00	0.24	9.6	5.7	2.41	96.1
28	LGR, NE, 1978	36.2	12.6	1.20	32.5	1.10	0.05	0.84	0.00	0.13	8.7	4.7	1.99	96.0
38	LGR, N, 1978	39.1	19.6	0.30	21.7	1.01	0.26	1.67	0.00	0.20	9.3	5.2	2.20	96.2
66	LGR, E, 1972	37.4	0.50	0.50	27.1	1.00	0.07	1.18	0.00	0.10	9.0	4.2	1.78	96.3
47	N of LGR	37.4	18.0	1.69	24.4	0.72	1.15	1.18	0.00	0.16	9.2	4.2	1.77	96.4
102, core	Wigwam Cr., SP	44.9	19.8	0.03	14.5	0.92	0.02	3.33	0.00	0.23	9.7	7.6	3.19	97.8
IV. Remnant, Early Miarolitic Cavity Mica; ferroan zinnwaldite														
72	LGR, 1986	43.4	20.5	0.15	15.8	0.66	0.50	2.90	0.00	0.05	10.0	6.3	2.63	97.6
73	LGR, 1986	42.7	19.9	0.54	16.5	0.62	0.47	2.70	0.00	0.10	10.0	6.1	2.58	97.1
V. Miarolitic Cavity; ferroan zinnwaldite, zinnwaldite, ferroan lepidolite														
104	Crystal Park area	44.6	20.5	0.10	13.0	0.79	0.10	3.25	0.00	0.13	10.3	8.0	3.36	97.5
106, core	Crystal Park area	44.2	20.2	0.14	14.9	0.40	0.01	3.13	0.00	0.08	10.1	7.3	3.08	97.4
106, rim	Crystal Park area	45.5	20.7	0.03	13.1	0.54	0.01	3.51	0.00	0.11	10.3	7.8	3.28	98.3
7	Devils Head	45.1	21.7	0.10	13.1	1.43	0.01	3.39	0.00	0.11	10.2	6.9	2.90	99.2
6, core	LGR, northern	41.1	22.3	0.04	17.3	1.74	0.30	2.24	0.00	0.20	9.4	5.5	2.30	97.8
6, rim	LGR, northern	40.6	20.7	0.85	18.3	1.18	0.73	2.10	0.00	0.12	9.8	5.1	2.17	97.3
77, core	LGR, 1986	43.5	20.4	0.38	15.7	0.62	0.41	2.93	0.00	0.07	10.0	7.1	3.01	98.1
77, rim	LGR, 1986	43.2	20.5	0.40	15.5	0.63	0.44	2.85	0.00	0.07	10.1	6.2	2.60	97.3
140	LGR	43.7	20.0	0.45	14.0	0.95	0.48	2.99	0.00	0.08	10.1	7.0	2.92	96.8
54, core	Harris Park area	44.7	20.9	0.26	13.9	1.24	0.21	3.28	0.00	0.13	10.2	6.9	2.91	98.8
54, rim	Harris Park area	46.1	20.9	0.10	12.4	1.20	0.18	3.68	0.00	0.09	10.2	7.6	3.20	99.3
114, rim	Sentinel Rock	51.3	18.7	0.02	7.8	0.65	0.02	5.17	0.00	0.04	10.3	9.8	4.14	99.7
124	Stove Mountain	45.6	21.3	0.01	13.2	0.64	0.00	3.53	0.00	0.05	10.0	9.0	3.78	99.5
4, core	Wigwam Cr., SP	45.7	20.6	0.02	14.0	0.84	0.08	3.56	0.00	0.27	9.8	7.9	3.31	99.5
4, rim	Wigwam Cr., SP	48.1	19.8	0.14	9.9	0.70	0.07	4.25	0.00	0.08	10.2	9.3	3.49	98.1
136, base	Wigwam Cr., SP	43.3	19.2	0.05	13.8	0.90	0.02	2.88	0.01	0.12	9.8	7.9	3.33	94.7
136, int.	Wigwam Cr., SP	48.4	19.8	0.14	9.8	0.65	0.04	4.34	0.00	0.10	10.5	9.7	4.10	99.3
136, rim	Wigwam Cr., SP	48.8	20.0	0.14	9.7	0.69	0.04	4.45	0.00	0.07	10.5	9.6	4.04	99.9
51, rim	Wigwam Cr., TH	45.4	21.5	0.03	12.4	1.25	0.00	2.71	0.00	0.14	10.7	8.0	3.36	98.8
VI. Miarolitic Cavity; muscovite														
112	Spruce Grove	44.8	27.7	0.09	10.2	0.41	0.04	-	0.00	0.10	10.6	2.7	1.15	95.5
146	Glen Cove	44.6	28.0	0.02	7.1	0.18	0.00	-	0.00	0.15	10.6	1.8	0.75	91.7

Li_2O calculated from $Li_2O = (0.287 \times SiO_2) - 9.552$ (Tindle & Webb, 1990).
Abbreviations: LGR = Lake George ring; RSG = Redskin Granite; SP = Sugarloaf Peak; TH = trailhead

analytical methods applied to mica is given by Wilcox (1984), who also summarized optical data for the different species of mica.

Electron-microprobe analyses were done at the U.S. Geological Survey in Denver using a JEOL 8900 Superprobe with five automated WDS spectrometers. Analyses were done using an accelerating voltage of 15 kV and a sample current of 20 nA. The following elements were sought: Na, Mg, Al, Si, Ca, Ti, Fe, F, Mn and K, using *K* lines in each case. Natural and synthetic mineral standards were used: albite (Na, Si), forsterite (Mg), anorthite (Al, Ca), rutile (Ti), fayalite (Fe), fluor-phlogopite (F), spessartine (Mn), and orthoclase (K). The concentration of Na, F, Al, Mg and Si was established using TAP crystals, that of K and Ca, using PET, and that of Fe, Mn and Ti, using LIF. For all elements except F, background counts were accumulated for 10 seconds and peak counts for 80 seconds; for F, background was accumulated for 40 seconds and peak for 80 seconds. Matrix corrections were performed using JEOL ZAF procedures. All but two samples were analyzed at 4 – 5 points each; samples 63 and 112 were analyzed at 2 and 6 points, respectively. Li content (not measured on account of small size of the samples) was calculated using a regression equation given by Tindle & Webb (1990) that is based on an empirical relation between Li_2O and SiO_2.

Relation of Optical Data to Composition

In the earliest comprehensive study of the relation between indices of refraction of a mica and its composition, Hall (1941) found n_γ to be related to the concentration of both Fe and Ti (with 1% TiO_2 causing an increase in n_γ of 0.0046), and also to the oxidation state of Fe (with Fe^{3+} giving a higher index than Fe^{2+}).

TABLE 4. EMPIRICAL FORMULAS FOR SELECTED MICAS FROM THE PIKES PEAK BATHOLITH

number	locality	Si	Al	Ti	Fe	Mn	Mg	Li	Ca	Na	K	F	SUM CATIONS
I. Host Granite; annite, biotite													
63	LGR, NE	5.60	2.46	0.49	4.44	0.07	0.55	0.25	0.00	0.02	1.86	0.46	15.74
68	LGR, SW	6.09	1.94	0.30	4.90	0.12	0.04	0.59	0.00	0.02	1.93	1.86	15.91
88	LGR, 1986	5.57	2.48	0.50	4.65	0.08	0.44	0.02	0.02	0.02	1.89	0.32	15.66
117	RSG, Tarryall	5.56	3.33	0.30	3.91	0.16	0.19	0.12	0.00	0.05	1.90	1.40	15.51
99	Wigwam Cr., SP	5.68	2.36	0.47	4.69	0.09	0.30	0.25	0.00	0.01	1.88	0.36	15.74
II. Graphic Pegmatite; biotite													
125	Crystal Park area	6.12	2.59	0.12	4.10	0.20	0.00	0.76	0.00	0.03	1.86	2.96	15.79
67	LGR, 1972	5.98	3.44	0.11	3.15	0.12	0.06	0.87	0.00	0.02	1.80	1.88	15.55
87	LGR, 1986	5.85	2.56	0.36	4.26	0.10	0.22	0.44	0.00	0.01	1.87	1.35	15.67
92	LGR, NE, 1978	6.11	2.53	0.14	4.23	0.13	0.02	0.76	0.00	0.03	1.84	2.02	15.79
65	N of LGR	5.99	3.44	0.18	2.76	0.08	0.22	1.01	0.00	0.04	1.82	2.04	15.55
98	Wigwam Cr., SP	5.84	2.63	0.19	4.69	0.19	0.00	0.33	0.00	0.03	1.87	1.85	15.77
III. Quartz Core; biotite													
103	Crystal Park area	6.24	3.25	0.06	2.77	0.10	0.05	1.25	0.00	0.07	1.90	2.79	15.69
28	LGR, NE, 1978	6.03	2.47	0.15	4.53	0.16	0.01	0.56	0.00	0.04	1.85	2.48	15.81
38	LGR, N, 1978	6.05	3.57	0.03	2.81	0.13	0.06	1.04	0.00	0.06	1.84	2.54	15.60
66	LGR, E, 1972	5.95	3.28	0.06	3.60	0.13	0.02	0.75	0.00	0.03	1.83	2.11	15.66
47	N of LGR	5.87	3.33	0.20	3.20	0.10	0.27	0.74	0.00	0.05	1.84	2.08	15.59
102, core	Wigwam Cr., SP	6.55	3.40	0.00	1.77	0.11	0.00	1.95	0.00	0.07	1.80	3.50	15.66
IV. Remnant, Early Miarolitic Cavity Mica; ferroan zinnwaldite													
72	LGR, 1986	6.36	3.54	0.02	1.94	0.08	0.11	1.71	0.00	0.01	1.87	2.92	15.65
73	LGR, 1986	6.33	3.48	0.06	2.05	0.08	0.10	1.61	0.00	0.03	1.89	2.86	15.63
V. Miarolitic Cavity; ferroan zinnwaldite, zinnwaldite, ferroan lepidolite													
104	Crystal Park area	6.52	3.53	0.01	1.59	0.10	0.02	1.91	0.00	0.04	1.92	3.70	15.64
106, core	Crystal Park area	6.48	3.49	0.02	1.83	0.05	0.00	1.85	0.00	0.02	1.89	3.39	15.63
106, rim	Crystal Park area	6.55	3.51	0.00	1.58	0.07	0.00	2.03	0.00	0.03	1.89	3.55	15.67
7	Devils Head	6.43	3.65	0.01	1.56	0.17	0.00	1.94	0.00	0.03	1.86	3.11	15.65
6, core	LGR, northern	6.08	3.89	0.00	2.14	0.22	0.07	1.33	0.00	0.06	1.77	2.57	15.68
6, rim	LGR, northern	6.07	3.65	0.10	2.29	0.15	0.16	1.26	0.00	0.03	1.87	2.41	15.59
77, core	LGR, 1986	6.37	3.52	0.04	1.92	0.08	0.09	1.73	0.00	0.02	1.87	3.29	15.63
77, rim	LGR, 1986	6.35	3.55	0.04	1.91	0.08	0.10	1.69	0.00	0.02	1.89	2.88	15.63
140	LGR	6.44	3.48	0.05	1.73	0.12	0.11	1.77	0.00	0.02	1.90	3.26	15.62
54, core	Harris Park area	6.43	3.54	0.03	1.67	0.15	0.05	1.90	0.00	0.04	1.87	3.14	15.67
54, rim	Harris Park area	6.55	3.50	0.01	1.47	0.14	0.04	2.10	0.00	0.02	1.85	3.41	15.68
114, rim	Sentinel Rock	7.06	3.03	0.00	0.90	0.08	0.00	2.86	0.00	0.01	1.81	4.27	15.76
124	Stove Mountain	6.52	3.59	0.00	1.58	0.08	0.00	2.03	0.00	0.01	1.82	4.07	15.62
4, core	Wigwam Cr., SP	6.53	3.47	0.00	1.67	0.10	0.02	2.04	0.00	0.07	1.79	3.57	15.69
4, rim	Wigwam Cr., SP	6.80	3.30	0.01	1.17	0.08	0.01	2.42	0.00	0.02	1.84	4.16	15.67
136, base	Wigwam Cr., SP	6.56	3.43	0.01	1.75	0.12	0.00	1.76	0.00	0.04	1.90	3.79	15.56
136, int.	Wigwam Cr., SP	6.81	3.28	0.01	1.15	0.08	0.01	2.46	0.00	0.03	1.88	4.32	15.72
136, rim	Wigwam Cr., SP	6.61	3.29	0.01	1.13	0.08	0.01	2.50	0.00	0.02	1.87	4.24	15.72
51, rim	Wigwam Cr., TH	6.54	3.65	0.00	1.49	0.15	0.00	1.57	0.00	0.04	1.97	3.65	15.42
VI. Miarolitic Cavity; muscovite													
112	Spruce Grove	6.38	4.65	0.01	1.21	0.05	0.00	-	0.00	0.03	1.93	1.22	14.26
146	Glen Cove	6.47	4.78	0.00	0.86	0.02	0.00	-	0.00	0.04	1.96	0.83	14.14

Empirical formulas based on 22 oxygens; iron computed as FeO; Li based on calculation after Tindle & Webb (1990).
Abbreviations: LGR = Lake George ring; RSG = Redskin Granite; SP = Sugarloaf Peak; TH = trailhead

Heinrich (1946) subsequently found a good correlation between n_γ and the concentration of Fe^{3+} and Ti. Rieder *et al.* (1971) later showed a correlation between indices of refraction and Fe in the sheets of octahedra in Li–Fe-rich micas, whereas Gottesmann & Tischendorf (1978) found the indices in trioctahedral micas to be proportional to the Fe^{2+} content, attaining maximum values with a simultaneously high Fe^{3+} content.

The suite of micas from the PPB in the present study shows an excellent linear relation between the total Fe (expressed as wt.% FeO) and n_β. Figure 8 gives a plot of total FeO *versus* n_β for selected samples from this study that have been quantitatively analyzed. The regression equation for these data is $y = 0.004725x + 1.519$ ($r^2 = 0.94$), where y is n_β and x is total Fe. A less precise correlation is noted between n_β and Ti ($r^2 = 0.83$), as well as between total Fe and $2V_x$, where the Fe content is generally inversely proportional to $2V_x$ ($r^2 = 0.35$). The relatively poor correlation between $2V_x$ and composition is presumably due to interlayering of twinned crystals (Bloss 1965, Axelrod & Grimaldi 1949), or to effects of polytypism (Rieder *et al.* 1971), either of which can lower the axial angle.

Zinnwaldite and ferroan lepidolite studied by Foord *et al.* (1995) are $1M$ polytypes, whereas lithian biotite was found either to be a $3T$ or $2M_1$ polytype; the single sample of muscovite consists of the $2M_1$ polytype. Sample 114 from this study (miarolitic-cavity zinnwaldite from Sentinel Rock) was determined by XRD to be a $1M$ polytype, whereas samples 129 and 147 (muscovite from Spruce Grove Campground and Glen Cove, respectively) were confirmed to be dioctahedral and to consist of the $2M_1$ polytype.

TABLE 5. INDEX OF REFRACTION β AND TOTAL Fe CONTENT FOR SELECTED OCCURRENCES OF MICA, PIKES PEAK BATHOLITH

number	mode	n_β	FeO
1986 Pegmatite, LGR			
88	host granite	1.705	33.3
87	graphic pegmatite	1.671	31.0
33	quartz core	1.667	nd
73	remnant mica	1.602	16.5
77	miarolitic cavity, core	1.599	15.7
72	remnant mica	1.597	15.8
77	miarolitic cavity, rim	1.589	15.5
56	miarolitic cavity	1.587	nd
74	miarolitic cavity	1.586	nd
Crystal Park			
103	quartz core	1.603	21.4
106	miarolitic cavity, core	1.583	14.9
106	miarolitic cavity, rim	1.580	13.1
North of LGR			
62	graphic pegmatite	1.641	24.0
66	quartz core	1.637	27.1
Harris Park			
54	miarolitic cavity, core	1.585	15.7
54	miarolitic cavity, rim	1.577	15.5
Wigwam Creek - Sugarloaf Peak			
99	host granite	1.697	34.2
98	graphic pegmatite	1.659	33.6
136	miar. cavity, base	1.586	13.8
102	quartz core, core	1.585	14.5
102	quartz core, rim	1.583	nd
4	miar. cavity, core	1.575	nd
136	miarolitic cavity, core	1.573	9.8
55	miarolitic cavity, core	1.572	nd
55	miarolitic cavity, rim	1.569	nd
136	miarolitic cavity, rim	1.569	9.7
4	miarolitic cavity, rim	1.567	9.9
Northeast of LGR, 1978			
90	host granite	1.703	nd
92	graphic pegmatite	1.657	30.9
28	quartz core	1.653	32.5
LGR, northern, 1978			
44	graphic pegmatite	1.655	nd
38	quartz core	1.623	21.7

The occurrences are listed in order of increasing n_β.

Sample 6 (Fig. 3), from a miarolitic cavity, is a high-Fe zinnwaldite to low-Fe biotite with a Ti-rich rim that shows higher indices of refraction for both core and rim than is typical for most cavity zinnwaldite. This is presumably due to its higher Fe and Ti content relative to other samples of zinnwaldite. The rim of this sample shows higher indices relative to the core, despite a lower Fe content in the rim; this is likely attributable to the substantially higher Ti content in the rim. This sample also shows a much lower $2V_x$ than expected, likely on account of its being a $3T$ polytype (determined by M.F. Brigatti, pers. commun., 1997).

Micas from the host Pikes Peak Granite have been defined as annite by Barker *et al.* (1975), on the basis of an average Fe content of 32.6% FeO. The high indices of refraction and Fe content for annite from the coarse-grained Pikes Peak Granite (Ypc) studied here (average n_β = 1.701 and 33.7 % FeO) fall within this range. The high index of refraction, compared to an upper limit of 1.690 given by Wilcox (1984), may be attributable to a compositional transition toward ferri-annite, which has a maximum n_β of 1.720 (Wilcox 1984). Optical data for miarolitic-cavity samples of zinnwaldite (average n_β = 1.579) fall well within published values, which range from 1.570 to 1.590 (Gottesmann & Tischendorf 1978, Němec 1983, Wilcox 1984). Optical properties for muscovite samples, with an average n_β of 1.595, are also within established values given by Wilcox (1984).

Figure 9 illustrates the relation between composition and n_β for selected constituents. This figure clearly shows the geochemical evolution of the micas, with decreasing FeO and TiO_2, and concomitantly increasing SiO_2, Al_2O_3, and F. K_2O (data not shown) shows a consistent value throughout the range of n_β.

Relation of Optical Data to Regional Geochemical Evolution

The relation between n_β and FeO (Fig. 8) and the correlation of Fe in mica with geochemical evolution in the PPB shown by Foord *et al.* (1995) permit the use

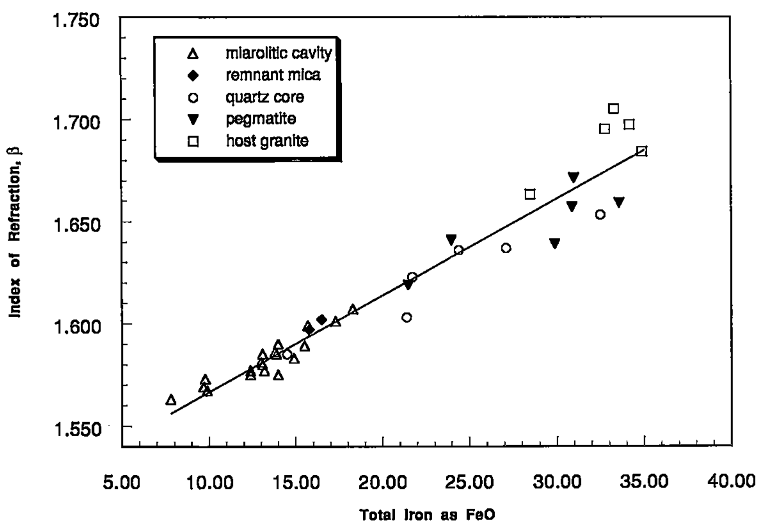

FIG. 8. Plot of iron content, expressed as wt% FeO, *versus* the β index of refraction of selected samples of mica.

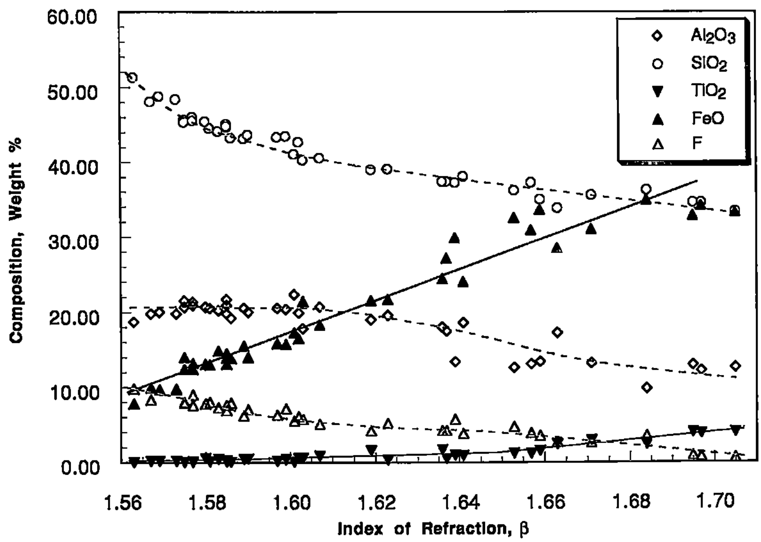

FIG. 9. Plot of β index of refraction *versus* composition, showing fractionation trend for selected constituents.

of optical data for an assessment of paragenesis. On a regional level, optical and compositional data of the micas illustrate a comparative geochemical evolution of granitic rocks within the PPB. For example, the lower n_β and FeO for a mica from the medium-grained granite composing a part of the Lake George ring complex (Ypm, sample 68), relative to those from the coarse-grained Pikes Peak Granite (Ypc), correlate with the later emplacement of this potassic pluton. Similarly, a mica from the Redskin Granite (sample 117), a highly evolved intrusive body (Hawley & Wobus 1977, Desborough *et al.* 1980), shows a considerably lower n_β (1.663) and FeO than do micas from the coarse-grained Pikes Peak Granite. The high degree of fractionation of the Redskin stock and associated pegmatites is further evidenced by the presence of muscovite in all three samples of miarolitic-cavity mica thus far studied.

Substantial differences in geochemical evolution are shown among pegmatites from different localities within the batholith. This is illustrated by comparatively low n_β and corresponding FeO values for quartz-core and miarolitic-cavity micas from the Sugarloaf Peak locality relative to similarly occurring micas from the 1986 locality in the Lake George ring complex. This finding suggests that intermediate stages of crystallization in the Sugarloaf Peak pegmatite are more highly evolved.

Optical and compositional data also correlate with mode of occurrence throughout the PPB, illustrating a progressive geochemical evolution from host granite → graphic pegmatite → quartz core → miarolitic cavity, with a general trend of decreasing indices of refraction and decreasing FeO (Fig. 8). The highest indices are found in mica from the host granite (average n_β = 1.693), and the lowest are represented by zinnwaldite to ferroan lepidolite (average n_β = 1.579) contained within miarolitic cavities. Although index of refraction (and FeO) is a more reliable indicator of mode of occurrence than is $2V_x$, the optic angle for micas from different modes of occurrence throughout the PPB is reasonably consistent, showing for the most part a low $2V_x$ expected for biotite and annite in granite, graphic pegmatite, and quartz-core occurrences, and a higher optic angle for the zinnwaldite – ferroan lepidolite from miarolitic cavities. Average values of optic angle for the micas shown in Table 2 range from 13.4° for host granite, 7.7° for graphic pegmatite, 9.5° for quartz core, and 28.4° for miarolitic-cavity zinnwaldite (calculated from rim samples where applicable, excluding sample 6), to 36.6° for miarolitic-cavity ferroan muscovite. Determinations of optic angle on 37 additional samples of mica (unpubl. data) corroborate these results.

Mica of intermediate composition, typical of quartz-core occurrences, has generally lower indices of refraction (average n_β = 1.631) compared to mica from surrounding pegmatites (average n_β = 1.654). However, the high n_β and corresponding FeO content for quartz-core micas compared to those in miarolitic cavities suggest a paragenetically earlier crystallization within the quartz core than in the miarolitic cavities. This sequence agrees with field observation, *e.g.*, late-formed minerals such as fluorite are not found enclosed in massive quartz, but early-formed species (such as zircon and ferrocolumbite) are. The final period of microcline crystallization within the quartz core was roughly contemporary with that of crystallization of the massive quartz, as shown by varying degrees of irregular surfaces (a result of growth interference) on microcline.

The greater range of $n_β$ (based on two standard deviations) for samples of quartz-core mica throughout the PPB (1.631 ± 0.029) relative to samples of miarolitic-cavity mica (1.579 ± 0.009) attests to a greater variability in degree of fractionation at the quartz-core stage of pegmatite development. Alternatively, the comparatively consistent $n_β$ for miarolitic-cavity micas throughout the PPB suggests a relatively uniform "endpoint" of geochemical evolution for the trioctahedral micas.

Paragenesis Within Individual Pegmatites

Although these optical and compositional data allow a comparison of geochemical differences for a given mode of occurrence among pegmatites from different localities, an unambiguous assessment of the paragenetic sequence within individual pegmatites can only be determined with data from proximate occurrences across a single pegmatite (*i.e.*, a cross-section through host granite, graphic pegmatite, quartz core, and miarolitic cavity). Figure 10 illustrates the relation between optical properties and paragenesis for four granitic pegmatites within the PPB, whereas Table 5 summarizes optical and compositional data for these and three other pegmatite cross-sections. Index of refraction, rather than % FeO, is shown in this figure because it was possible to obtain a complete set of data throughout the pegmatite cross-sections. Although this figure shows overlapping ranges of index of refraction ($n_β$) in mica samples from the quartz core and graphic pegmatite zones from different localities, there is nevertheless a continuous evolutionary trend within a given pegmatite toward a lower $n_β$ index. Figure 10 further illustrates the early paragenesis of mica in the quartz core relative to the miarolitic-cavity stage of crystallization.

The consistent decrease in index of refraction within a series of mica samples from a pegmatite is not always paralleled by a decrease in FeO (Table 5), but the discrepancies fall within limits of analytical error. Such discrepancies may also be attributable to electron-microprobe data acquired on slightly altered or limonite-coated mica grains, whereas polarized light microscopy, by virtue of a better visual estimate of such features, seems to give more consistent results.

A complete evolutionary trend, from host granite to miarolitic cavity, is illustrated by a series of mica samples from the Sugarloaf Peak and the 1986, Lake George ring-complex localities. Specimens from both occurrences show a progressive decrease in $n_β$ (and corresponding decrease in FeO) throughout the sequence of crystallization. The Sugarloaf Peak (Wigwam Creek) occurrence is an extensive, zoned, nearly horizontal pegmatite that exceeds 100 m in length; it is more than 1 m thick in places, with numerous quartz lenses and small miarolitic cavities occurring throughout the structure. The high degree of evolution of micas in quartz-core and miarolitic-cavity occurrences in this pegmatite (shown by their low values of $n_β$), relative to other localities such as the 1986 pegmatite (discussed in detail below), is clearly illustrated in Figure 10. It is important to note that although the above data show consistent evolutionary trends within individual pegmatites throughout the PPB, they also illustrate fundamental differences in evolution among different pegmatites as well as pegmatite districts.

Remnants of early-formed, partly resorbed micas line the walls of small irregular cavities or depressions that remain following partial to nearly complete dissolution of the original crystal. These small voids, typically situated near the base of microcline crystals or in the graphic pegmatite wallrock adjacent to the miarolitic cavity, retain their original, usually irregular pseudohexagonal form, typically with a characteristic lining of quartz microcrystals. The "remnant" flakes retain their original orientation in the nearly hollow cavity, *i.e.*, with (001) being perpendicular to the long axis of the cavity. Optical properties of such mica (samples 72, 73, and 153) substantiate their early formation in the miarolitic cavity, and suggest a paragenesis that is equivalent to the early polycrystalline core of mica crystals from other pegmatites, *e.g.*, samples 54 and 77.

The last stages of fractionation within individual miarolitic cavities are shown by zoned crystals of zinnwaldite (samples 4, Fig 2; 54, Fig. 6; 77 and 106) that show a decrease in $n_β$ and FeO from core to rim. Electron-microprobe traverses across three zoned crystals of miarolitic-cavity zinnwaldite show a fluctuating Ti content that closely correlates with color zonation (darker zones have higher Ti), whereas total iron shows a consistent decrease from core to rim (unpubl. data). Later stages of sequential differentiation are particularly well represented by the specimen shown in Figure 11, from the Sugarloaf Peak locality. This specimen (sample 136) exhibits a continuous sequence of mica crystallization with a corresponding decrease in $n_β$ and FeO, from a polycrystalline base ($n_β$ = 1.586, FeO = 13.8%) partly enclosed by graphic pegmatite, to an epitactic open-cavity zinnwaldite that shows zonation from a brown interior ($n_β$ = 1.573, FeO = 9.8%) to a pale-brown rim ($n_β$ = 1.569, FeO = 9.7%).

Paragenesis of the 1986 Pegmatite

A detailed example for the geochemical evolution of mica within a single body of pegmatite is provided by an occurrence in the coarse-grained Pikes Peak Granite (Ypc) near the Lake George ring complex, in

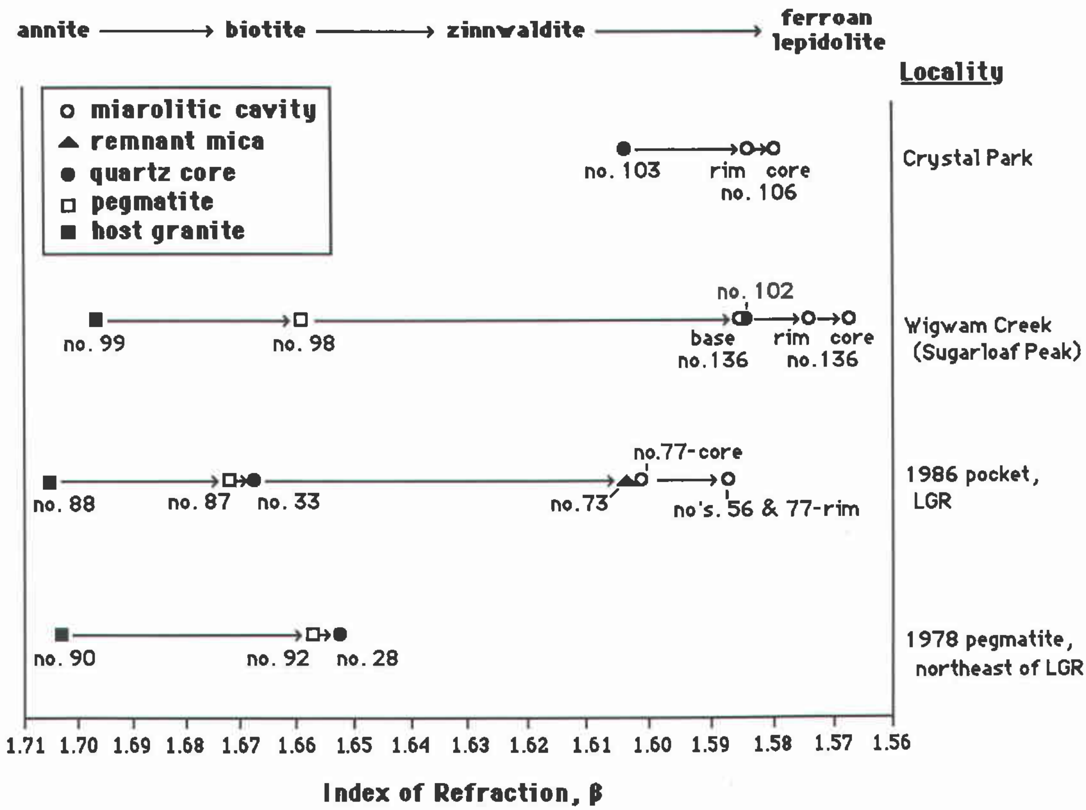

FIG. 10. Sequential differentiation of micas through cross-sections within individual pegmatites in the Pikes Peak batholith. The figure shows optical progression in the sequence host granite → graphic pegmatite → quartz core → miarolitic cavity. Sample numbers given on plot; LGR: Lake George ring complex.

FIG. 11. Matrix specimen from Sugarloaf Peak, Wigwam Creek area, illustrating early-generation polycrystalline mica (showing evidence of partial dissolution) that is partly enclosed by the wallrock of the miarolitic cavity, and later-generation, open-cavity epitactic growth of monocrystalline, zoned zinnwaldite (sample no. 136, Table 2), associated with microcline, variety amazonite. Specimen is 11 cm across.

which the presence of mica in all modes of occurrence within the pegmatite, and comprehensive field data, allow a complete assessment of its paragenesis. A diagram of this pegmatite is shown in Figure 12; it illustrates a miarolitic cavity, adjacent bodies of massive quartz, and surrounding granite; mica sample locations also are indicated. Figures 13 and 14 illustrate *in situ* cross-sectional views of this occurrence. This pegmatite, excavated in 1986, represents a zonal structure and mineralogy that are characteristic of the Crystal Peak area.

Paragenesis of minerals adjacent to and within the miarolitic cavity is shown in Figure 15. Amazonitic microcline, albite, and biotite are enclosed by massive quartz at the extremities of the elongate miarolitic cavity. The massive quartz becomes increasingly fragmented and more loosely consolidated toward the pocket margin, with large partial prism faces of milky to gray quartz facing the adjacent cavity. Crystallization within the central miarolitic cavity consisted of early amazonitic microcline and platy albite, followed by extensive crystallization of euhedral quartz that formed mostly on the ceiling of the pocket. Later-formed minerals within the cavity include (in paragenetic order) fluorite, hematite, and calcite.

The mica samples collected from this pegmatite and surrounding host granite (summarized in Table 5) show a progressive decrease in n_β and FeO, from annite in the host granite, to biotite in the pegmatite and quartz core, to ferroan zinnwaldite and zinnwaldite in the miarolitic cavity. The decrease in index of refraction and FeO suggests that the formation of the massive quartz and its enclosed mica (and feldspar minerals) at the distal ends of this pegmatite preceded major crystallization in the centrally located miarolitic cavity. Formation of the euhedral quartz crystals in the miarolitic cavity is not likely to have been either earlier than or contemporary with the formation of the massive quartz because: (1) massive quartz is not seen enclosing late-formed fluorite crystals, (2) mica crystals enclosed in massive quartz have higher indices of refraction (and a corresponding higher Fe content) than those within the miarolitic cavity, and (3) euhedral quartz crystals (*i.e.*, smoky quartz) do not enclose biotite, but commonly partly enclose crystals of zinnwaldite and amazonitic microcline.

Remnant ferroan zinnwaldite, showing an optic angle and indices of refraction intermediate to those of biotite and zinnwaldite, was noted as minute flakes (sample 72) on the walls of an irregular cavity alongside the base of a microcline crystal, and as fragments (sample 73) in an elongate depression (showing part of the original pseudohexagonal outline) in massive quartz and microcline adjacent to the miarolitic cavity. Continuing fractionation within the miarolitic cavity is shown by a distinct zonation between the core and rim of sample 77, evidenced by decreasing n_β and increasing $2V_x$. This zonation is possibly a result of a pocket-rupture event (shown in Fig. 15); broken quartz crystals that show varying degrees of regrowth as well as the presence of fine-grained crystals also are probable manifestations of one or more pocket-rupture events.

A Proposed Model of Evolution for Pegmatites of the Pikes Peak Batholith

Studies of pegmatite genesis [Jahns & Burnham (1969), Jahns (1979, 1982), London (1986, 1990, 1992)] have established two general models for the development of miarolitic-cavity-bearing pegmatites. These are largely based on studies of LCT-type pegmatites in the Peninsular Ranges batholith of southern California. Few studies, however, have focused on miarolitic-cavity-bearing pegmatites of the PPB (*e.g.*, Wobus *et al.* 1988). The optical and compositional data presented here, as well as field evidence, provide new details concerning the evolution of pegmatite bodies and miarolitic cavities in the PPB, and are in agreement with the major tenets of the general models proposed in earlier research. Much of this proposed model is based on the early crystallization of massive quartz, which has specific implications regarding pegmatite genesis.

This model of evolution postulates that graphic pegmatites formed within fracture zones of the granite that were caused by tensional features related to the emplacement of late plutons within the parent granite. Attitude and configuration of the fractures, and of the resultant bodies of pegmatite, likely played a role in the development of late-stage mineralization. Irregularities in inclination may have facilitated entrapment of a residual fluid phase that exsolved from the silicate melt as it crystallized during cooling of the parent granite. Segregation and coalescence of vapor within the pegmatite-forming melt resulted in the appearance of miarolitic cavities. In the PPB, miarolitic cavities are most abundant in pegmatites with dips less than about 30°, but rare in vertical or near-vertical pegmatites, from which the volatiles presumably more readily escaped. It is possible, however, that some miarolitic cavities noted in steeply inclined pegmatites formed as a result of escaping volatiles that were trapped either at an interface, such as a diorite porphyry, or at a granodiorite xenolith caprock (Wobus *et al.* 1988). Alternatively, it is possible that early crystallization of massive quartz within the miarolitic cavities formed a constriction that trapped the volatile phase, which may account for cavities seen in many pegmatites in the PPB that show no conspicuous inflection in dip. This is in contrast to the pegmatite dikes of San Diego County, California, where pegmatite configuration appears to be a controlling factor for the location of miarolitic cavities.

Whereas crystallization of massive quartz adjacent to miarolitic cavities preserved the enclosed biotite, crystals of ferroan zinnwaldite that subsequently

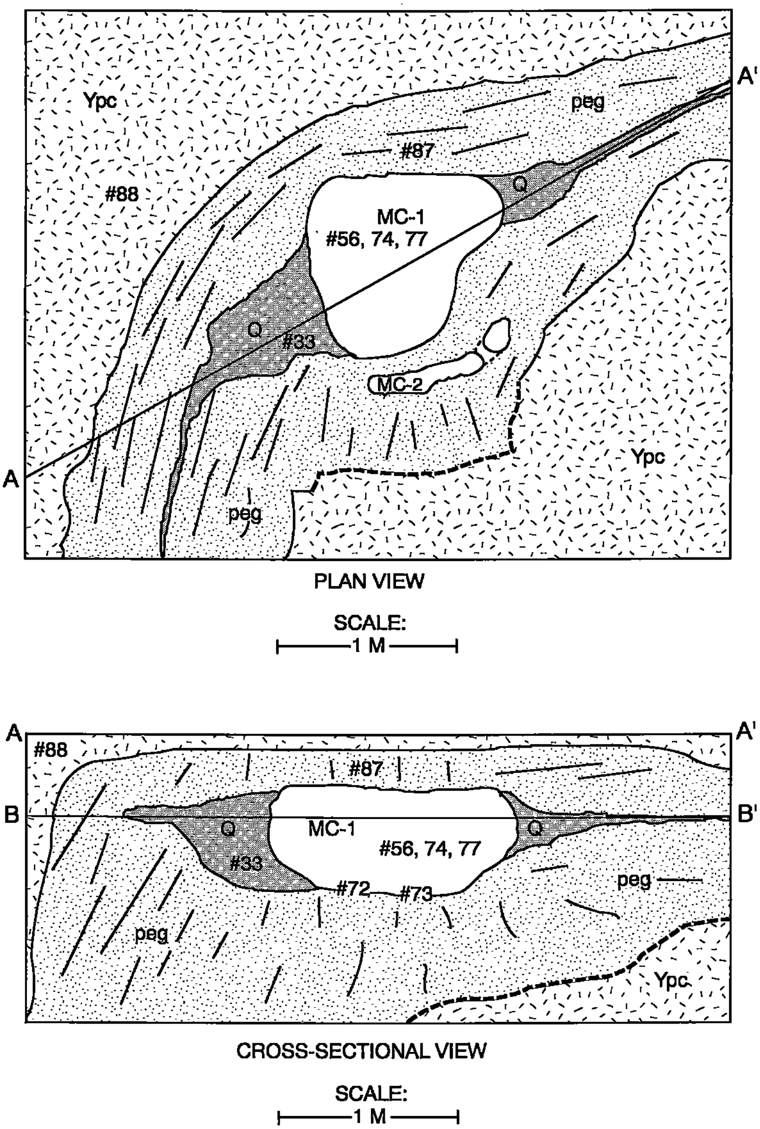

FIG. 12. Diagram of a pegmatite with enclosed miarolitic cavity and adjacent massive quartz, excavated near the Lake George ring complex in 1986. Ypc: coarse-grained Pikes Peak Granite, peg: pegmatite showing graphic structure near cavity border, Q: massive quartz, MC: miarolitic cavity. The position of mica samples collected from within this pegmatite is indicated by sample numbers in the diagram. Boundaries dashed where inferred. A–A': line of cross-section, B–B': level of exposure for plan view.

FIG. 13. Cross-sectional view of miarolitic cavity with surrounding pegmatite illustrated in Figure 12. Field of view approximately 1.5 m across.

FIG. 14. Close-up view of miarolitic cavity shown in Figure 13. Detached crystals of microcline, variety amazonite, and smoky quartz are seen partly enclosed by pocket clay. Field of view approximately 0.6 m across.

formed early within the remaining central miarolitic cavities and adjacent wallrock were resorbed to varying extents, leaving pseudohexagonal cavities that may contain remnant mica. The instability of the early-cavity mica may result from increased pressure within the miarolitic cavity and concomitant changes in oxygen fugacity, partial pressures of H_2O, and activities of chemical constituents in the vapor phase, all of which have been shown to affect the composition and field of stability of micas in silicate melts (Eugster 1957, Eugster & Wones 1958, 1962, Peikert 1963, Wones & Eugster 1965, Rieder 1971, Syritso *et al.* 1996). This increase in pressure likely resulted from exsolution of an aqueous vapor phase due to crystallization of the silicate melt (Burnham 1979a, b, 1983). Internal pressures exceeding lithostatic pressure could have resulted in pocket rupture and a subsequent reduction in pressure that would cause abrupt changes

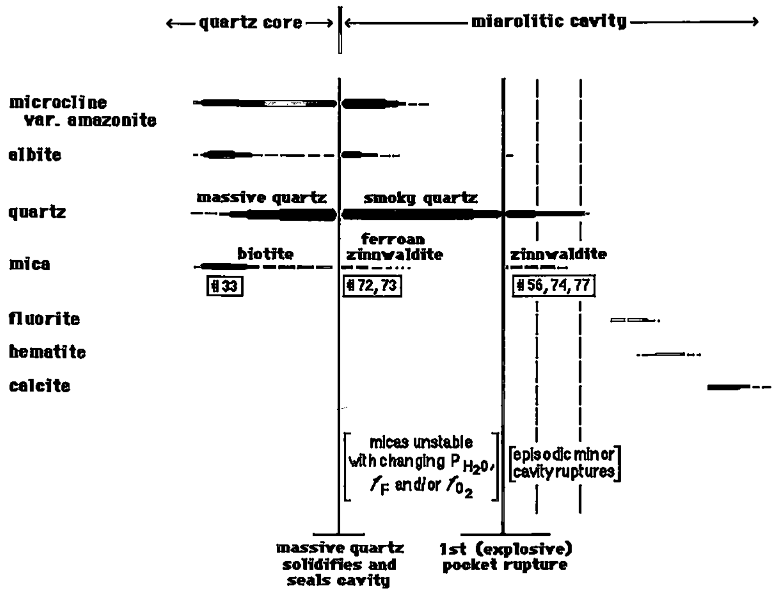

FIG. 15. Paragenetic sequence of minerals in the 1986 pegmatite. Position of specific samples of mica within this sequence is indicated by sample numbers in the figure. Dashed lines represent inferred events of pocket rupture in the miarolitic cavity.

in fluid composition (*e.g.*, Fe and Ti) and account for some of the simple zonation seen in mica. However, the presence of numerous such zones within a small linear span (*e.g.*, Figs. 5, 7), which suggests rapid compositional changes within a relatively short time, is likely due to a chemical diffusion process initiated by crystallization.

The model proposed here requires that a silicate melt phase persists throughout most of the crystallization from aqueous fluid within the miarolitic cavity to account for continuing generation of pressure. Coexistence of a silicate melt with an aqueous vapor phase at temperatures compatible with formation of α-quartz may be possible under metastable, disequilibrium conditions (London *et al.* 1989, London 1992, 1996), or in the presence of F [found at an average concentration of 0.47% in the Pikes Peak Granite by Hawley & Wobus (1977)]. Fluorine is known to reduce the solidus of granitic systems (Manning 1981, London *et al.* 1989, London 1992).

SUMMARY AND CONCLUSIONS

The composition of mica provides an excellent indicator of geochemical differentiation within the PPB. Because the index of refraction of the micas shows a close linear relation to FeO (which is correlated to the degree of fractionation of the magma), determination of n_β can provide an unambiguous assessment of paragenesis on both regional and local scales.

A continuum of fractionation, based on indices of refraction and composition of the micas, is shown throughout the PPB, from the least-evolved pegmatites in the Lake George ring complex, to the ferroan lepidolite-bearing pegmatite in the Sugarloaf Peak (Wigwam Creek) area, and ultimately to the muscovite-bearing pegmatites at Glen Cove and within the Redskin Stock. The transition of mica composition, from quartz-enclosed biotite crystals at the distal ends of the miarolitic cavity, to resorbed crystals of ferroan zinnwaldite at the margin of the cavity, and finally to euhedral, late-formed zinnwaldite to ferroan lepidolite within the miarolitic cavity, substantiates a sequence of crystallization from the quartz core inward toward the adjacent miarolitic cavity. Crystallization within miarolitic cavities represents the final stage of fractionation, and reaches a uniform compositional "endpoint", as evidenced by the relatively consistent value of n_β and FeO content of the trioctahedral mica in the miarolitic cavities. Crystallization within the cavities ceased when the silicate melt was exhausted and the vapor phase was depleted of all dissolved constituents.

The general sequence of development of miarolitic cavities proposed here is partly based on cavity-rupture events due to the hydrostatic pressure exerted by the aqueous phase that results from closed-system crystallization from the silicate melt phase, with subsequent resealing and continuing crystallization. This model accounts for the simple zonation of pocket mica and the shock damage and regrowth of other crystals. It is in agreement with the models advanced by Jahns (1979, 1982), largely based on studies of pegmatite bodies in San Diego County, California, and by London (1990, 1992, 1996). However, additional details are added that are specific to the PPB pegmatites, *i.e.*, the early crystallization of massive quartz that may account (in part) for the formation of miarolitic cavities and results in closed-system conditions. It should be noted that some aspects of paragenesis, as expressed in the above model, may not apply to all pegmatite occurrences in the PPB, but general elements of this model should be pertinent to miarolitic-cavity-bearing pegmatites throughout the PPB. Details of the paragenetic sequence will vary depending on local conditions of formation, such as attitude and size of the pegmatite, and local variations in composition of the silicate melt and aqueous fluids. Although this model of pegmatite paragenesis contradicts aspects of an earlier report, in which the quartz core mode was postulated to be the last-formed phase within a pegmatite (Wobus *et al.* 1988), field evidence, and optical and compositional data reported here appear to best support the proposed interpretation.

Finally, it appears that polarized light microscopy provides an economical and reliable method for assessing geochemical evolution in igneous bodies, particularly if one must rely on partly altered samples.

ACKNOWLEDGEMENTS

The authors thank Ray Berry, Roger Bennett, Joe Dorris, George Fisher, Nik Golosow, Bill Hayward, Bruce Kinney, Bryan Lees, Lee McKinney, Tom Michalski, Jack Murphy (Denver Museum of Natural History), Larry Piekenbrock, Jack Thompson, and Dan Unruh (U.S. Geological Survey) for providing some of the mica samples used in this study. William B. Simmons and Alexander U. Falster (University of New Orleans), B.F. Leonard and Tom Michalski (U.S. Geological Survey), Petr Černý (University of Manitoba), Mickey Gunter (University of Idaho), André Lalonde (University of Ottawa), and an anonymous reviewer provided technical reviews of the manuscript. We also thank William B. Simmons (University of New Orleans), David London (University of Oklahoma), Peter J. Modreski (U.S. Geological Survey), Stephen Guggenheim (University of Illinois), and F. Donald Bloss (Virginia Polytechnic Institute and State University) for helpful discussions and suggestions regarding aspects of pegmatite paragenesis, mica structure, and optical measurements. M.F. Brigatti (University of Modena, Italy) kindly provided the polytype determination for sample no. 6.

REFERENCES

AXELROD, J.M. & GRIMALDI, F.S. (1949): Muscovite with a small optic axial angle. *Am. Mineral.* **34**, 559-572.

BARKER, F., WONES, D.R., SHARP, W.N. & DESBOROUGH, G.A. (1975): The Pikes Peak batholith, Colorado Front Range, and a model for the origin of the gabbro – anorthosite – syenite – potassic granite suite. *Precamb. Res.* **2**, 97-160.

BLASI, A., BRAJKOVIC, A., DE POL BLASI, C., FOORD, E. E., MARTIN, R.F. & ZANAZZI, P.F. (1984): Structure refinement and genetic aspects of a microcline overgrowth on amazonite from Pikes Peak batholith, Colorado, U.S.A. *Bull. Minéral.* **107**, 411-422.

BLOSS, F.D. (1965): Pitfall in determining $2V$ in micas. *Am. Mineral.* **50**, 789-792.

BRYANT, B., MCGREW, L.W. & WOBUS, R.A. (1981): Geologic map of the Denver 1° × 2° quadrangle, north-central Colorado. *U.S. Geol. Surv., Map* **I-1163**.

BURNHAM, C.W. (1979a): The importance of volatile constituents. *In* The Evolution of Igneous Rocks (H.S. Yoder, Jr., ed.). Princeton University Press, Princeton, New Jersey (439-482).

________ (1979b): Magmas and hydrothermal fluids. *In* Geochemistry of Hydrothermal Ore Deposits (2nd edition, H.L. Barnes, ed.). J. Wiley & Sons, New York, N.Y. (71-136).

________ (1983): Deep submarine pyroclastic eruptions. *In* The Kuroko and Related Volcanogenic Massive Sulfide Deposits (H. Ohmoto & B.J. Skinner, eds.). *Econ. Geol., Monogr.* **5**, 142-148.

ČERNÝ, P. (1991): Rare-element granitic pegmatites. I. Anatomy and internal evolution of pegmatite deposits. *Geosci. Can.* **18**, 49-67.

DESBOROUGH, G.A., LUDINGTON, S.D. & SHARP, W.N. (1980): Redskin Granite: a rare-metal-rich Precambrian pluton, Colorado, USA. *Mineral. Mag.* **43**, 959-966.

EUGSTER, H.P. (1957): Stability of annite. *Carnegie Inst. Wash., Yearbook* **56**, 161-164.

________ & WONES, D.R. (1958): Phase relations of hydrous silicates with intermediate Mg/Fe ratios. *Carnegie Inst. Wash., Yearbook* **57**, 193-194.

________ & ________ (1962): Stability relations of the ferruginous biotite, annite. *J. Petrol.* **3**, 82-125.

FOORD, E.E., ČERNÝ, P., JACKSON, L.L., SHERMAN, D.M. & EBY, R.K. (1995): Mineralogical and geochemical evolution of micas from the miarolitic pegmatites of the anorogenic Pikes Peak batholith, Colorado. *Mineral. Petrol.* **55**, 1-26.

________ & MARTIN, R.F. (1979): Amazonite from the Pikes Peak batholith. *Mineral. Rec.* **10**, 373-384.

GOTTESMANN, B. & TISCHENDORF, G. (1978): Klassification, Chemismus und Optik trioktaedrischer Glimmer. *Z. Geol. Wiss. Berlin* **6**, 681-708.

HALL, A.J. (1941): The relation between chemical composition and refractive index in the biotites. *Am. Mineral.* **26**, 34-41.

HAWLEY, C.C. (1969): Geology and beryllium deposits of the Lake George (or Badger Flats) beryllium area, Park and Jefferson counties, Colorado. *U.S. Geol. Surv., Prof. Pap.* **608-A**.

________ & WOBUS, R.A. (1977): General geology and petrology of the Precambrian crystalline rocks, Park and Jefferson counties, Colorado. *U.S. Geol. Surv., Prof. Pap.* **608-B**.

HEINRICH, E.W. (1946): Studies in the mica group; the biotite – phlogopite series. *Am. J. Sci.* **244**, 836-848.

HUTCHINSON, R.M. (1976): Granite-tectonics of the Pikes Peak batholith, Colorado. *In* Studies in Colorado Field Geology (R.C. Epis & R.J. Weimer, eds.). *Colorado School of Mines, Prof. Contrib.* **8**, 32-43.

________ (1988): Granite tectonics of the Pikes Peak composite batholith, Colorado. *In* Field Trip Guidebook (G.S. Holden, ed.). *Colorado School of Mines, Prof. Contrib.* **12**, 47-58.

JAHNS, R.H. (1979): Gem-bearing pegmatites in San Diego County, California: the Stewart mine, Pala district, and the Himalaya mine, Mesa Grande district. *In* Mesozoic Crystalline Rocks: Peninsular Ranges Batholith and Pegmatites Point Sal Ophiolite (P.L. Abbott & V.R. Todd, eds.). *Geol. Soc. Am., Field Trip Guidebook*, 3-38.

________ (1982): Internal evolution of granitic pegmatites. *In* Granitic Pegmatites in Science and Industry (P. Černý, ed.). *Mineral. Assoc. Can., Short Course Handbook* **8**, 293-327.

________ & BURNHAM, C.W. (1969): Experimental studies of pegmatite genesis. I. A model for the derivation and crystallization of granitic pegmatites. *Econ. Geol.* **64**, 843-864.

LONDON, D. (1986): Formation of tourmaline-rich gem pockets in miarolitic pegmatites. *Am. Mineral.* **71**, 396-405.

________ (1990): Internal differentiation of rare-element pegmatites; a synthesis of recent research. *In* Ore-Bearing Granite Systems; Petrogenesis and Mineralizing Processes (H.J. Stein & J.L. Hannah, eds.). *Geol. Soc. Am., Spec. Pap.* **246**, 35-50.

________ (1992): The application of experimental petrology to the genesis and crystallization of granitic pegmatites. *Can. Mineral.* **30**, 499-540.

________ (1996): Granitic pegmatites. *Trans. R. Soc. Edinburgh, Earth Sci.* **87**, 305-319.

________, MORGAN, G.B., VI & HERVIG, R.L. (1989): Vapor-undersaturated experiments with Macusani glass + H_2O at 200 MPa, and the internal differentiation of granitic pegmatites. *Contrib. Mineral. Petrol.* **102**, 1-17.

MANNING, D.A.C. (1981): The effect of fluorine on liquidus phase relationships in the system Qz–Ab–Or with excess water at 1 Kb. *Contrib. Mineral. Petrol.* **76**, 206-215.

NĚMEC, D. (1983): Zinnwaldite in moldanubischen Lithium-Pegmatiten. *Chem. Erde* **42**, 197-204.

PEIKERT, E.W. (1963): Biotite variation as a guide to petrogenesis of granitic rocks in the Pre-Cambrian of northeastern Alberta. *J. Petrol.* **4**, 432-459.

RIEDER, M. (1971): Stability and physical properties of synthetic lithium-iron micas. *Am. Mineral.* **56**, 256-280.

________, PÍCHOVÁ, A., FASSOVÁ, M., FEDIUKOVÁ, E. & ČERNÝ, P. (1971): Chemical composition and physical properties of lithium-iron rich micas from the Krušné hory (Erzgebirge), Czechoslovakia and Germany. B. Cell parameters and optical data. *Mineral. Mag.* **38**, 190-196.

SIMMONS, W.B., LEE, M.T. & BREWSTER, R.H. (1987): Geochemistry and evolution of the South Platte granite–pegmatite system, Jefferson County, Colorado. *Geochim. Cosmochim. Acta* **51**, 455-471.

SYRITSO, L.F., PONOMAREVA, N.I. & BUTORIN, V.V. (1996): Physical-chemical conditions of stability for Li–Fe micas in rare-metal granites. *Zap. Vses. Mineral. Obshchest.* **125**(1), 73-80 (in Russ.).

TINDLE, A.G. & WEBB, P.C. (1990): Estimation of lithium contents in trioctahedral micas using microprobe data: application to micas from granitic rocks. *Eur. J. Mineral.* **2**, 595-610.

UNRUH, D.M., SNEE, L.W., FOORD, E.E. & SIMMONS, W.B. (1995): Age and cooling history of the Pikes Peak batholith and associated pegmatites. *Geol. Soc. Am., Abstr. Programs* **27**, A-468.

WILCOX, R.E. (1984): Optical properties of micas under the polarizing microscope. *In* Micas (S.W. Bailey, ed.). *Rev. Mineral.* **13**, 183-200.

WOBUS, R.A. (1986): The Pikes Peak batholith and associated plutons. *In* Colorado Pegmatites: Abstracts, Short Papers, and Field Guides from the Colorado Pegmatite Symposium (P.J. Modreski, ed.). Colorado Chapter, Friends of Mineralogy, 70-71.

________ & ANDERSON, R.S. (1978): Petrology of the Precambrian intrusive center at Lake George, southern Front Range, Colorado. *U.S. Geol. Surv., J. Res.* **6**, 81-94.

________, FINNEMORE, S. & SMITH, D. (1988): Geology of the Ten Percenter mine, Lake George district, Teller County, Colorado. *In* Field Trip Guidebook (G.S. Holden, ed.). *Colorado School of Mines, Prof. Contrib.* **12**, 43-46.

________ & HUTCHINSON, R.M. (1988): Proterozoic plutons and pegmatites of the Pikes Peak region, Colorado. *In* Field Trip Guidebook (G.S. Holden, ed.). *Colorado School of Mines, Prof. Contrib.* **12**, 35-42.

WONES, D.R. & EUGSTER, H.P. (1965): Stability of biotite: experiment, theory, and application. *Am. Mineral.* **50**, 1228-1272.

Received April 25, 1996, revised manuscript accepted February 21, 1998.